Journal of Catalysis 279 (2011) 75–87

Contents lists available at ScienceDirect

Journal of Catalysis

journal homepage: www.elsevier.com/locate/jcat

Vital roles of hydroxyl groups and gold oxidation states in Au/ZrO_2 catalysts for 1,3-butadiene hydrogenation

Xin Zhang [a,b], Hui Shi [a,1], Bo-Qing Xu [a,*]

[a] Innovative Catalysis Program, Key Lab for Organic Optoelectronics & Molecular Engineering, Department of Chemistry, Tsinghua University, Beijing 100084, China
[b] State Key Laboratory of Heavy Oil Processing, China University of Petroleum, Changping, Beijing 102249, China

ARTICLE INFO

Article history:
Received 17 September 2010
Revised 31 December 2010
Accepted 4 January 2011
Available online 18 February 2011

Keywords:
Gold nanoparticles
Hydrogenation catalysis
ZrO_2
Butadiene
Surface hydroxyls
Gold oxidation state
Active sites

ABSTRACT

Hydrogenation of 1,3-butadiene over Au/ZrO_2 catalysts with different gold loadings and calcination temperatures was reported. The catalysts were characterized in depth to understand their structure–property relationship. Gold oxidation states and surface hydroxyl groups, which were found to be sensitive to the gold loading, calcination temperature, and treatment with water, were shown to play vital roles in the hydrogenation activity of Au/ZrO_2. Continued activity decrease was seen when the density of surface hydroxyl groups was lowered by elevating the pre-calcination temperature of ZrO_2. Fully dehydroxylated Au/ZrO_2 was essentially inactive, but became very active after partial regeneration of the hydroxyl groups by water treatment. Moreover, the activity of Au/ZrO_2 increased with increasing Au^{3+}/Au^0 ratio. Isolated Au^{3+} ions at the support surface showed up to two orders of magnitude higher activity than Au^0 atoms on Au particles. Several models are proposed to address the structural features of active sites for H_2 activation in Au/ZrO_2 catalysts.

1. Introduction

Supported gold catalysts have unexpectedly been found to be active for a wide variety of reactions [1]; however, most of the studies have been devoted to the unprecedented activity of nano-sized gold catalysts for CO oxidation. The nature of active sites and reaction mechanisms for CO oxidation on gold catalysts has been extensively studied [1–6]. In contrast, little work has been done to gain insight into the activity and nature of gold catalysts for hydrogenation reactions [7,8], especially for the hydrogenation of unsaturated hydrocarbons [9–13], in spite of some elegant documentation on gold-catalyzed hydrogenation of α,β-unsaturated aldehydes/ketones [14–18]. This is surprising, since catalytic hydrogenation represents a well-studied and industrially important category of chemical reactions on conventional transition metal catalysts [19].

Supported gold catalysts prepared by the conventional impregnation method were found to show very low catalytic rates for the hydrogenation of unsaturated hydrocarbons in the 1970s [9,10]. The first report was made by Bond et al. [9], who investigated impregnated Au/SiO_2 and $Au/\gamma\text{-}Al_2O_3$ catalysts for the hydrogenation of 1-pentene, 1,3-butadiene, and 2-butyne. These authors speculated, without direct evidence, that the hydrogenation activity of their gold catalysts arose from small gold particles having a large number of defects, or resided in even smaller particles not witnessed by electron microscopy. Buchanan and Webb [10] studied the reaction of 1,3-butadiene with H_2/D_2 over Au/Al_2O_3 catalysts with widely varied Au sizes. They claimed that the special sites capable of activating molecular hydrogen would reside in extremely small gold particles not sensed by their electron microscopy. Due to the limitations of the impregnation method for preparing gold catalysts (e.g., wide Au size distribution and possible contamination by poisonous chloride residues [1,4,12]), these earlier attempts to understand the catalytic sites might be severely distorted. Using improved preparation methods (e.g., deposition–precipitation), Au nanoparticles on oxide supports were prepared and tested as catalysts for the hydrogenation of unsaturated hydrocarbons [12,13]. For the hydrogenation of acetylene over Au/Al_2O_3, a maximum reaction rate was observed over the sample having an average Au particle size of 3 nm [13]. For hydrogenation of 1,3-butadiene, however, the reaction rates over oxide-supported Au catalysts appeared almost insensitive to the Au particle size as well as to the nature of the oxide supports [12].

In contrast to the well-established knowledge of H_2 chemisorption/activation over Group VIII metals (e.g., Pd, Pt), H_2 chemisorption/activation on supported gold catalysts is far from clear. Chemisorption of H_2 molecules does not occur on clean "bulky" gold surfaces but is occasionally reported on supported small gold nanoparticles [7,11,20,21]. Theoretical calculations of H_2 activation

* Corresponding author. Fax: +86 10 6279 2122.
E-mail address: bqxu@mail.tsinghua.edu.cn (B.-Q. Xu).
[1] Present address: Department Chemie, Technische Universität München, Lichtenbergstr. 4, D-85748 Garching, Germany.

0021-9517/$ - see front matter © 2011 Elsevier Inc. All rights reserved.
doi:10.1016/j.jcat.2011.01.002

by dissociation on single-crystal Au surfaces or gold clusters with varying numbers of Au atoms provide some information [22–24], but these theoretical models can be far from real catalysts and sometimes produce controversial results. It should be pointed out that these earlier experimental and/or theoretical assessments of H_2 chemisorption and hydrogenation reactions were in most cases done on supported metallic gold catalysts, which could have neglected possible involvements of cationic gold species and the underlying support surfaces in H_2 activation.

For CO oxidation [25–28] and water–gas shift reactions [29], cationic gold species (Au^{3+} and/or Au^{+}) sometimes are found to be superior to metallic gold (Au^0), at least on several oxide supports. The first demonstration of high activity of immobilized Au^{3+} ions for olefin hydrogenation was documented using MgO-supported mononuclear Au (III) complex catalyst for ethene hydrogenation [30]. It was clearly shown with in situ X-ray absorption near-edge structure (XANES) that mononuclear Au^{3+} complexes, but not metallic gold clusters, were responsible for the hydrogenation activity [30]. We previously communicated that isolated Au^{3+} ions on a ZrO_2 surface were highly active for the selective hydrogenation of 1,3-butadiene [27,31]. These cationic gold species were also found to be active for olefin (propene) hydrogenation [32]. These results are encouraging, which identified that immobilized surface cationic gold species have potential as new catalyst for the hydrogenation of unsaturated hydrocarbons, even though H_2 could potentially be a reducing agent to the cationic gold species.

It was reported that moisture (water vapor) in the reaction feed or in some cases hydroxyl groups on the catalyst surface [33,34] could influence the catalytic activity of oxide-supported gold for CO oxidation. Nevertheless, effects of moisture and surface hydroxyl groups on the gold-catalyzed hydrogenation of unsaturated hydrocarbons have not yet been explored. Here, a series of Au/ZrO_2 catalysts, with different gold loadings and calcination temperatures, are prepared by deposition–precipitation and investigated for the selective hydrogenation of 1,3-butadiene. A detailed analysis of the catalyst structure is provided, based on characterizations using a variety of techniques. We attempt to gain insight into the structure–performance relationship for 1,3-butadiene hydrogenation over these Au/ZrO_2 catalysts. Particular attention is paid to the effects of moisture in the reaction feed, density of hydroxyl groups on the support surface, and percentage of Au^{3+} species in gold. Several model structures are envisaged to discuss the structural features of active sites in Au/ZrO_2 catalysts.

2. Experimental

2.1. Catalyst preparation

Two kinds of zirconia were prepared, using $ZrO(OH)_2$ hydrogel obtained by hydrolysis of zirconyl chloride in aqueous ammonia, as described previously [5,35]. Following our earlier sample coding, ZrO_2-CP-*t* denotes the sample prepared by calcination for 5 h in flowing air of the $ZrO(OH)_2$ hydrogel at temperature t = 673, 873, 973 and 1073 K, respectively. A $ZrO(OH)_2$ alcogel was prepared by extensive washing with anhydrous ethanol of the $ZrO(OH)_2$ hydrogel [35]. A follow-up calcination for 5 h of the $ZrO(OH)_2$ alcogel in flowing N_2 at temperature t produced the ZrO_2-AN-*t* samples.

Zirconia-supported gold catalysts were prepared using a deposition–precipitation method. Briefly, zirconia powders (2 g) were added into an appropriate amount of aqueous $HAuCl_4$ solution. The solution pH was adjusted to ca. 9 by controlled addition of 0.2 M $NH_3{\cdot}H_2O$ solution. The aqueous dispersions were stirred for 6 h, aged for 2 h, and suction filtered. Extensive washing with deionized water was then continued until it was free of Cl^- ions. Conductivity of the final filtrate was less than 10^{-5} S m^{-1}. The samples were dried at 393 K overnight and then calcined in flowing air (60 ml min^{-1}) at temperature T for 5 h (ramp rate: 10 K min^{-1}). The samples were denoted as Au/ZrO_2-CP(AN)-*t*-*T*. *t* refers again to the pre-calcination temperature of ZrO_2 support (before gold was loaded) and *T* is the catalyst calcination temperature (after gold was loaded). Unless specified, the actual gold loadings were between 0.63 and 0.76 wt.% by ICP-AES analysis, but the nominal gold loading in the preparation was 1.0 wt.% for these Au/ZrO_2-CP-*t*-*T* and -AN-*t*-*T* samples. Variation in gold loading in the range of 0.01–1.0 wt.% was intentionally made within the Au/ZrO_2-CP-673-473 samples, by adjusting the amounts of aqueous $HAuCl_4$ during the deposition–precipitation stage; these samples are labeled as *m*%Au/ZrO_2-CP-673-473 and *m*% denotes the actual gold loading by weight percentage. In addition, a 0.08%Au/ZrO_2-CP-673-473 was prepared by treatment of the Au/ZrO_2-CP-673-473 (1.0% nominal Au loading) with a 2% KCN solution as described previously [31].

2.2. Catalyst characterizations

The catalysts were characterized by a number of techniques including XRD, TEM, XPS, TPR, ESR, IR, TG-DTA, N_2 adsorption, and element analysis (ICP-AES), the details of which are given in the Supplementary material. H_2-TPD measurements were performed on a TPR apparatus [31] equipped with both TCD and MS (Balzers MSC 200) detectors. Typically, the catalyst sample (200 mg for 0.05%Au/ZrO_2-CP-673-473, 100 mg for the others) was put into a U-shaped quartz reactor (i.d. 4 mm) and pretreated in flowing Ar at the catalyst calcination temperature *T* for 1 h. After the sample was cooled to 393 K (the reaction temperature of 1,3-butadiene hydrogenation), the reactor was switched to H_2 flow (45 ml min^{-1}) for 1 h. The reactor was then switched back to Ar and purged for 0.5 h, followed by cooling to room temperature. TCD and MS (m/z = 2) signals were recorded when the reactor was heated from room temperature up to 1073 K at a rate of 10 K min^{-1} in flowing Ar (45 ml min^{-1}).

2.3. Catalytic hydrogenation of 1,3-butadiene

Hydrogenation of 1,3-butadiene was carried out at 393 K in a fixed-bed flow stainless reactor (i.d. 6 mm) under atmospheric pressure. Unless otherwise specified, the reaction feed was a gas mixture of 2.15 vol.% 1,3-butadiene in H_2, which was introduced into the reactor at a space velocity (GHSV) of 8100 ml h^{-1} (g cat.)$^{-1}$. The catalyst (ca. 100 mg Au/ZrO_2 in 80–120 mesh) was diluted with 500 mg of quartz sand before being loaded into the reactor. Before it was switched to the reaction feed gas, the catalyst was pretreated in flowing Ar (30 ml min^{-1}) at 473 K for 2 h. The reaction conditions were similar to those applied by Okumura et al. [12]. In some experiments, a 0.05%Au/ZrO_2-CP-673-473 catalyst was pretreated with flowing H_2 (30 ml min^{-1}) at 473 or 523 K for 2 h to investigate the effect of hydrogen reduction on catalyst activity; the reduced catalyst was then cooled to 393 K in flowing Ar (30 ml min^{-1}) to evaluate its catalytic activity for the hydrogenation reaction. Any significant mass-transfer limitation was precluded in a series of pre-experiments at a fixed space velocity (e.g., GHSV = 8100 ml h^{-1} (g cat.)$^{-1}$) so that the conversion of 1,3-butadiene over a highly active Au/ZrO_2 catalyst was not significantly affected by changing the flow rate of the reaction feed and the catalyst pellet size in 40–120 mesh. The reactor effluent was analyzed on line using a GC-8A gas chromatograph equipped with a GDX-501 column and a FID detector.

To study the effect of moisture on the hydrogenation reaction, the reaction feed gas was set to pass through a glass vessel (250 ml) containing ca. 50 g H_2O. The temperature was varied

between 203 and 273 K in order to change the concentration of moisture (gaseous H_2O) in the range of 20–6000 ppm. The reaction feed in these experiments was a gas mixture composed of 1,3-butadiene, H_2, and N_2 with a volumetric ratio of 1:49:97 and was introduced at a GHSV of 23,820 ml h^{-1} (g cat.)$^{-1}$.

3. Results

3.1. Physicochemical properties of zirconia support

Fig. 1A shows TG/DTA curves for the $ZrO(OH)_2$ hydrogel and its derived alcogel. Mass spectroscopic analyses of the effluent gas during the TG/DTA process of the hydrogel are shown in Fig. 1B. The weight loss between 323 and 450 K on the TG curve can be generally ascribed to the desorption of weakly adsorbed water molecules. Further weight loss at above 450 K would be associated with the desorption of strongly adsorbed water and/or dehydration by surface dehydroxylation [36]. The DTA curve of the $ZrO(OH)_2$ hydrogel shows a weak but broad endothermic peak ranging from 323 to 673 K, due to the water desorption and dehydration by surface dehydroxylation. The sharp exothermic peak at 719 K on the DTA curve of the hydrogel is known as the glow exotherm associated with the formation of crystalline zirconia [37]. An additional exothermic feature was observed at a lower temperature (634 K) on the DTA curve of the alcogel. This new peak would arise from the decomposition and/or combustion of surface ethoxy groups, which agrees with the detected evolutions of H_2O, CH_3CHO/CO_2, and C_2H_4 (m/z = 18, 44, 28, and 27) as shown in Fig. 1B. The weight loss on the TG curve for the alcogel (22.1%) was more than twice that for the hydrogel (10.5%), which demonstrated that the preparation of $ZrO(OH)_2$ alcogel by repeated washing of the $ZrO(OH)_2$ hydrogel with anhydrous ethanol induced significant replacement

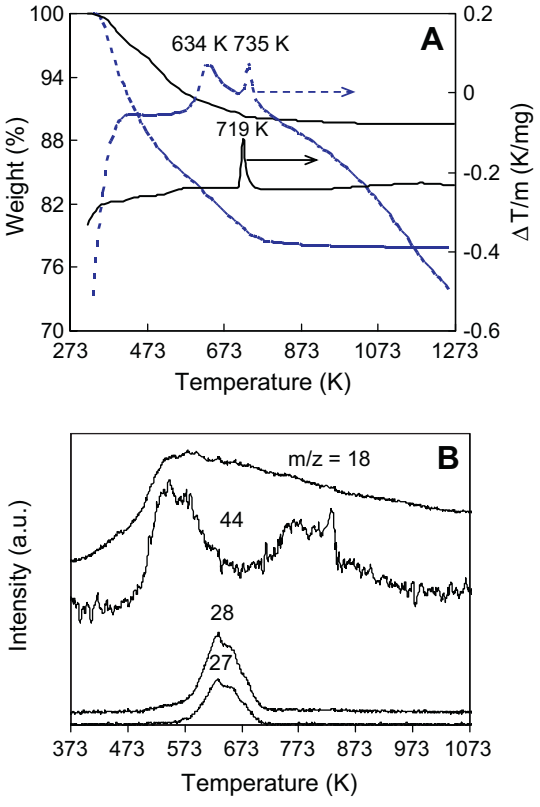

Fig. 1. (A) TG/DTA curves of $ZrO(OH)_2$ hydrogel (solid line) and its derived alcogel (dotted line); (B) mass spectroscopic analyses of the effluent gas from the alcogel during TG/DTA.

of the hydroxyl groups (HO—, formula mass 17) in the original gel with ethoxyl groups (CH_3CH_2O—, formula mass 45) in ethanol: $(—OH)_s + CH_3CH_2OH \rightarrow (—OCH_2CH_3)_s + H_2O$, leading to formation of surface ethoxyls in the alcogel [38]. Therefore, the density of surface hydroxyl groups would be higher on a ZrO_2 sample obtained from the $ZrO(OH)_2$ hydrogel (ZrO_2-CP) than on the sample obtained from its derived $ZrO(OH)_2$ alcogel (ZrO_2-AN) using the same calcination procedure. In other words, the ZrO_2-AN-*t* sample would carry fewer hydroxyl groups than ZrO_2-CP-*t*. As can be judged from the TG curves, the density of hydroxyl groups for both ZrO_2-AN-*t* and -CP-*t* samples would decrease with *t*. The undetectable weight loss from the TG curves in the range 1073–1273 K would suggest that nearly fully dehydroxylated ZrO_2 samples can be prepared by calcination of $ZrO(OH)_2$ at a temperature as high as 1073 K.

The textural properties of ZrO_2-CP-*t* and -AN-*t* are summarized in Table 1. Nitrogen adsorption measurements show that BET surface areas of ZrO_2-CP-*t* are 120, 44, 23, and 14 m^2 g^{-1} at t = 673, 873, 973, and 1073 K, respectively. These surface area data are close to those documented earlier by Nakano et al. [39]. In comparison with ZrO_2-CP-*t*, much higher surface areas and pore volumes were observed for ZrO_2-AN-*t* (Table 1). XRD patterns (see Fig. S1 in the Supplemental material) show that the present ZrO_2 samples are all composed of monoclinic (M) and tetragonal (T) phases [5]. The phase composition of ZrO_2-CP-*t* and -AN-*t* when *t* was higher than 873 K could not be differentiated (Table 1). Although the average crystal sizes determined by the X-ray line broadening analysis (XLBA) seemed similar for ZrO_2-CP-*t* and -AN-*t* when *t* was less than 1073 K, the average domain sizes of ZrO_2-AN-*t* particles in TEM images appeared much smaller than those of their ZrO_2-CP-*t* counterparts. The similar particle sizes obtained from XLBA and TEM measurements for the ZrO_2-AN-*t* would hint that these samples were composed of discrete ZrO_2 nanocrystals. In contrast, the difference between the XLBA and TEM sizes of the conventional ZrO_2-CP-*t* would indicate that the primary crystallites in these samples agglomerated more or less into larger particles. We believe that the transformation of the conventional $ZrO(OH)_2$ hydrogels to its alcogels can reduce the capillary pressure and density of hydroxyl groups in the gel network, because the surface tension of ethanol would be much lower than that of water (22.39 vs 72.88 dyn/cm at 293 K), which could endow the alcogel-derived ZrO_2-AN sample with greater resistance to structure collapse and thermal sintering [38,40].

3.2. Physicochemical properties of zirconia-supported gold catalysts

3.2.1. Textural and morphologic properties

ICP-AES analyses showed that zirconia-supported gold samples contained ca. 0.70% (in the range 0.63–0.76%), 0.23%, 0.05%, and 0.01% gold by weight, corresponding to nominal gold loadings of 1.0%, 0.25%, 0.05%, and 0.01%, respectively. Nitrogen adsorption measurement showed that the deposition of gold had little impact on the texture properties of zirconia as long as the catalyst calcination temperature *T* remained no higher than 473 K. The BET surface areas of the Au/ZrO_2-CP-673-*T* catalysts decreased from 100 to 74 m^2 g^{-1} when *T* was increased from 573 to 773 K (Table 2). XRD patterns of the Au/ZrO_2 catalysts were found similar to those of their corresponding "pure" ZrO_2 supports; no diffraction associated with gold was observed.

Fig. 2 shows some representative TEM/HRTEM images for the Au/ZrO_2-CP-*t*-*T* samples (the images for Au/ZrO_2-AN-***t***-673 samples were given elsewhere [5]). As can be seen in Fig. 2A, our careful search for Au particles in the HRTEM images for *m*%Au/ZrO_2-CP-673-473 samples at gold loadings of 0.01%, 0.05%, and 0.08% always produced negative results, which would indicate that gold in these samples was atomically dispersed on the zirconia support surface. This agrees with Fu et al. [29], who showed that

Table 1
Texture properties of ZrO_2-CP-*t* and ZrO_2-AN-*t* samples.

Sample	BET surface area (m^2/g)	Pore volume (cm^3/g)	Average pore size (nm)	XLBA size[a] (nm)	TEM size (nm)	ZrO_2-phase[a] (%)
ZrO_2-CP-673	120	0.16	3.9	M6/T5	10–30	M54/T46
ZrO_2-CP-873	44	0.12	8.5	M12/T11	30–100	M88/T12
ZrO_2-CP-973	23	0.11	16.3	M22	40–200	M92/T8
ZrO_2-CP-1073	14	0.07	14.5	M40	40–200	M98/T2
ZrO_2-AN-673	162	0.36	6.7	M6/T5	5–10	M76/T24
ZrO_2-AN-873	61	0.28	15.3	M12/T11	12–17	M88/T12
ZrO_2-AN-973	36	0.26	24.8	M21	20–25	M92/T8
ZrO_2-AN-1073	20	0.19	33.9	M30	25–40	M97/T3

[a] M and T represent monoclinic and tetragonal phases, respectively.

Table 2
Physicochemical properties and catalytic activity of Au/ZrO_2 catalysts in selective hydrogenation of 1,3-butadiene.

Catalyst	BET surface (m^2/g)	d_{Au} (nm)	OH (mmol/g)	Red. temp. (K)	H_2 uptake[a]	Au^{3+}/Au^0	Conv. (%)	Rxn. rate (mmol s^{-1} (g Au)$^{-1}$)	TOF[b] (s^{-1})
Au/ZrO_2-AN-1073-673	18	3.0–7.0 (5.4)	–	–	0	0	3.0	–	–
Au/ZrO_2-AN-973-673	34	3.0–7.0 (4.7)	–	–	0	0	12.0	0.03	0.03
Au/ZrO_2-AN-873-673	53	3.0–7.0 (4.7)	–	–	0	0	18.0	0.05	0.04
Au/ZrO_2-AN-673-673	142	3.0–7.0 (5.4)	–	–	0	0	49.0	0.13	0.10
Au/ZrO_2-CP-1073-473	14			424	0.14	0.10	19.0	0.05	0.04 (0.11)
Au/ZrO_2-CP-1073-573	14			–	0	0	3.4	–	–
Au/ZrO_2-CP-1073-673	14	7–13 (10.0)	0.23 (0.30)[c]	–	0	0	2.6	–	–
Au/ZrO_2-CP-973-673	22	3.0–7.0 (4.0)	0.38	–	0	0	8.8	0.02	0.01
Au/ZrO_2-CP-873-673	34	4.0–8.3 (6.2)	0.68	–	0	0	32.0	0.09	0.09
Au/ZrO_2-CP-673-773	74	6.5–13.4 (11.7)	–	–	0	0	6.8	0.02	0.03
Au/ZrO_2-CP-673-673	90	5.6–10.4 (8.0)	0.75	–	0	0	39.0	0.10	0.12
Au/ZrO_2-CP-673-573	100	4.5–9.0 (6.7)	–	488	0.25	0.20	53.4	0.14	0.17 (0.17)
Au/ZrO_2-CP-673-473	100	3.0–7.0 (4.1)	–	483	0.37	0.33	75.2	0.20	0.17 (0.16)
Au/ZrO_2-CP-673-393	100	2.5–5.5 (3.5)	–	483	0.44	0.42	98.4	0.38	0.31 (0.25)
0.23%Au/ZrO_2-CP-673-473	110	2.0–4.0 (2.9)	–	482	0.68	0.83	39.3	0.34	0.17 (0.16)
0.08%Au/ZrO_2-CP-673-473	–	n.d.[d]	–	496	1.50	∞[e]	85.4	2.15	(0.42)
0.05%Au/ZrO_2-CP-673-473	120	n.d.[d]	–	504	1.49	∞[e]	49.9	2.01	(0.40)
0.01%Au/ZrO_2-CP-673-473	120	n.d.[d]	–	508	1.57	∞[e]	10.3	2.08	(0.41)

[a] The unit is mol(H_2)/mol(Au).
[b] The TOF data were calculated on the basis of exposed Au^0 atoms or Au^{3+} ions (data in the parentheses) in the catalyst.
[c] Data in the parentheses is the hydroxyl concentration of 0.74% Au/ZrO_2-CP-1073-673 treated with deionized water.
[d] n.d.: undetectable in the HRTEM measurement.
[e] Only Au^{3+} ions were found.

0.5% Au/Ce(La)O_2 obtained by subjecting their 5% Au/Ce(La)O_2 catalyst to an aqueous solution of 2% NaCN contained only atomically dispersed gold species. Nearly spherical Au particles were observed for the Au/ZrO_2-CP-673-*T* samples; their average size became greater and their size distribution wider when *T* was increased from 393 to 773 K. For comparison, Au particles in those Au/ZrO_2-AN-*t*-673 samples (Table 2) showed a relatively narrower size distribution (3–7 nm) and a smaller average sizes (4–5 nm) [5].

3.2.2. Assessment of surface hydroxyl groups

The Au/ZrO_2-CP-*t*-673 samples were characterized with IR spectroscopy to compare their hydroxyl groups. Fig. 3 shows the IR spectra in the —OH stretching vibration region. Three absorption bands at around 3770, 3680, and 3630 cm^{-1} were observed on Au/ZrO_2-CP-673-673. It was understood that weakly adsorbed water molecules (or coordinated molecular water) on highly hydrated zirconia surfaces could be eliminated easily upon evacuation at 450 K, but hydroxyl groups on the same surfaces were sustained up to ca. 873 K [36]. Because all the samples were pretreated in situ at 450 K in vacuum for 1 h to remove any coordinated water molecules before their IR spectra were recorded, it would be impossible to relate the broad peak at around 3680 cm^{-1} to a presence of molecularly absorbed water. The three peaks of Fig. 3a are then assigned to terminal and bi- and tri-bridged hydroxyl groups, respectively [41]. The terminal hydroxyl groups (ca. 3770 cm^{-1}) were sharply weakened when *t* was increased from 673 to 873 K and became invisible when *t* was increased to 973 K or higher. The increase in *t* also significantly reduced the adsorption bands for bi- (ca. 3680 cm^{-1}) and tri-bridged hydroxyl groups (ca. 3630 cm^{-1}). Ultimately, the surface of Au/ZrO_2-CP-1073-673 (Fig. 3d) showed basically no sign of any of those hydroxyl groups. Interestingly, simple water treatment of this hydroxyl-free Au/ZrO_2-CP-1073-673 sample resulted in partial regeneration of all three kinds of surface hydroxyl groups (Fig. 3e), due to rehydration of the support oxide.

The number of hydroxyl groups was evaluated by TG measurements of the Au/ZrO_2-CP-*t*-673 samples, which were pretreated in situ at 673 K (473 K for the water-treated Au/ZrO_2-CP-1073-673) in flowing dry air for 0.5 h. The numbers were 0.75, 0.68, 0.38, and 0.23 mmol/g for Au/ZrO_2-CP-*t*-673 samples with *t* = 673, 873, 973, and 1073 K, respectively (Table 2). We found that the number for Au/ZrO_2-CP-1073-673 increased from 0.23 to 0.30 mmol/g after it was treated with water, in accordance with the observed regeneration of surface hydroxyls after the water treatment in the IR measurements. These results clearly show that the concentration of hydroxyl groups in Au/ZrO_2 catalysts depends sensitively on the support calcination temperature *t*.

3.2.3. Oxidation states of Au/ZrO_2 catalysts

Fig. 4 shows the XPS spectra of Au4*f* in Au/ZrO_2-CP-673-*T* samples. Compared with the Au4$f_{7/2}$ and 4$f_{5/2}$ binding energies (BEs) for both *T* = 673 and 773 K samples (Fig. 4d and e), the Au XPS peaks for the *T* = 393, 473, and 573 K samples (Fig. 4a–

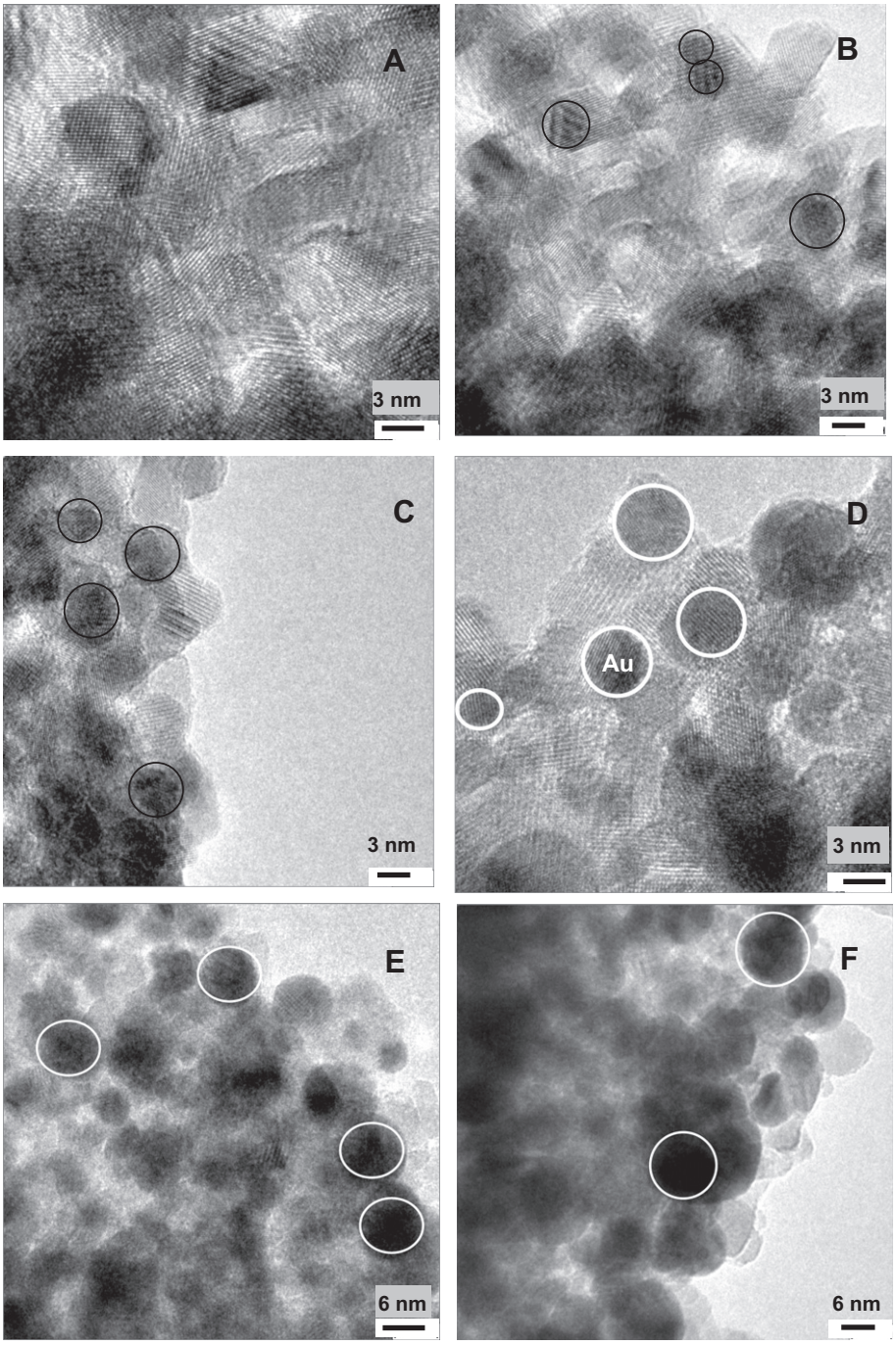

Fig. 2. Representative TEM/HRTEM images of Au/ZrO_2-CP-*t*-*T* catalysts: (A) Au/ZrO_2-CP-673-473 containing 0.01%, 0.05%, and 0.08% Au by weight; (B) 0.23%Au/ZrO_2-CP-673-473; (C) Au/ZrO_2-CP-673-393; (D) Au/ZrO_2-CP-673-473; (E) Au/ZrO_2-CP-673-573; (F) Au/ZrO_2-CP-673-673; (G) Au/ZrO_2-CP-673-773; (H) Au/ZrO_2-CP-873-673; (I) Au/ZrO_2-CP-973-673; (J) Au/ZrO_2-CP-1073-673.

c) showed significantly higher BEs (by up to ca. 1.0 eV). The BEs at 83.6 and 87.4 eV for both $T = 673$ and 773 K samples were characteristic of metallic Au [5,26]. The higher Au4*f* BEs for the samples with $T < 673$ K could easily be attributed to the presence of cationic gold species (Au^{3+} or/and Au^{+}). However, it is understood that quantitative assessment of the gold oxidation state by XPS characterization alone is limited because the final state effects associated with particle size could heavily disturb the XPS features of Au [6,25,42] and the exposure to photoelectrons under high vacuum during XPS measurement might also effect change in the gold oxidation state [25,43]. In principle, the Auger parameter can be used to check the electronic nature by the initial state effects, but the high kinetic energies of the relevant Auger electrons would make it difficult to measure supported gold nanoparticles; an earlier attempt made by Hutchings et al. [25] failed in obtaining valuable information even for a 5% Au/Fe_2O_3 catalyst because of poor signal intensity.

We recognize that it is more reliable to titrate the oxidation states of gold using quantitative H_2-TPR, as shown in earlier literature [27,31,44,45]. Fig. 5A shows the TPR profiles for Au/ZrO_2-CP-673-*T* of varying gold loadings. The profiles for the samples with $T = 393$, 473, and 573 K featured two hydrogen consumption peaks, one in low (482–508 K)- and the other in high (ca. 830 K)-temperature regions. It is known that a sufficiently high calcination

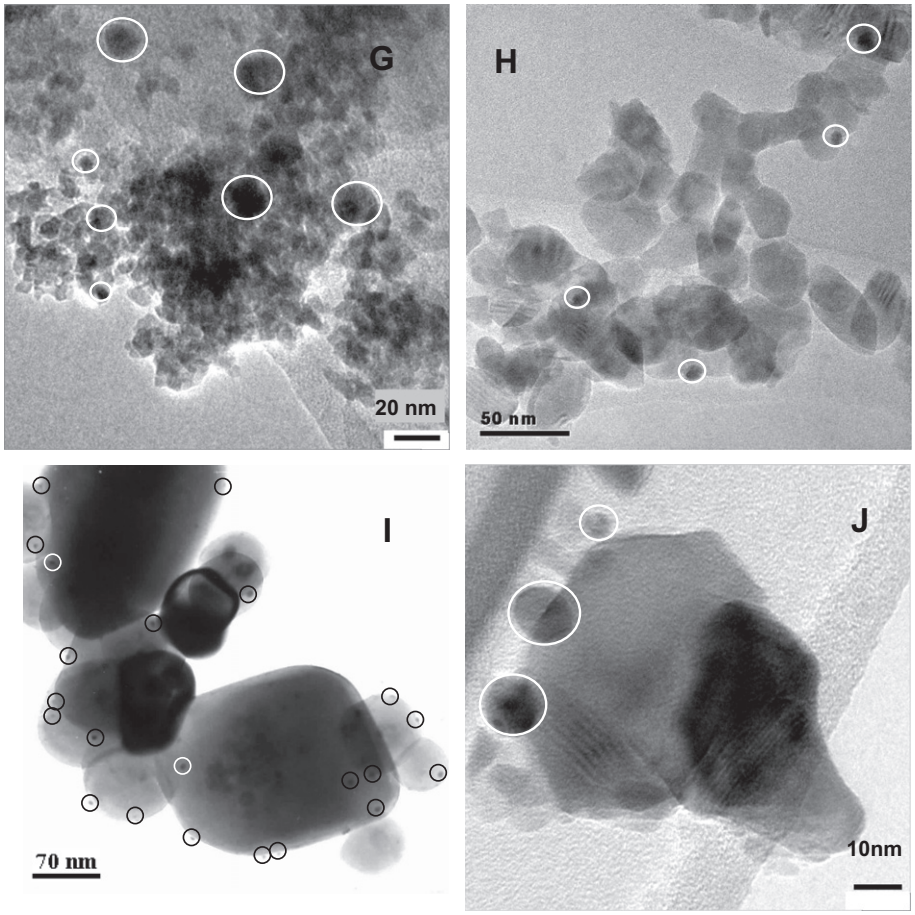

Fig. 2 (*continued*)

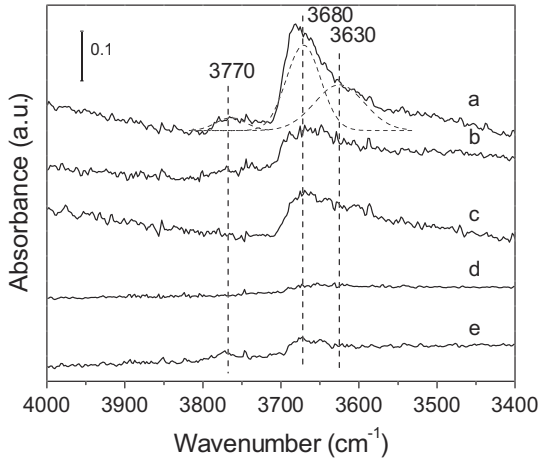

Fig. 3. Infrared spectra of hydroxyl groups on Au/ZrO_2-CP-*t*-673 of *t* = 673 (a), 873 (b), 973 (c), and 1073 K (d), and the water-treated Au/ZrO_2-CP-1073-673 (e).

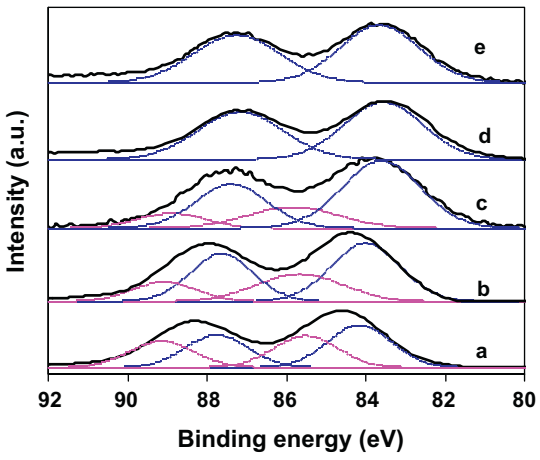

Fig. 4. XPS spectra of Au4*f* in Au/ZrO_2-CP-673-*T* samples of *T* = 393 (a), 473 (b), 573 (c), 673 (d), and 773 K (e).

temperature (generally no less than 673 K) would induce complete decomposition/reduction of the cationic species to metallic gold particles [25–27]. This point is confirmed here by our observation that no reduction of cationic gold could be detected for the *T* = 673 K sample. Thus, the low-temperature peak would be related to a reduction of cationic gold species, while the high-temperature one would be related to a partial (<3%) reduction of Zr^{4+} to Zr^{3+} in the support oxide [31,45].

The calibrated hydrogen consumption data disclosed that the stoichiometry for the hydrogen reduction of gold was H_2/Au (molar) = 1.50 ± 0.2 for the Au/ZrO_2-CP-673-473 samples containing no more than 0.08% gold. This stoichiometry clearly shows that Au^{3+} ions were the only gold species in the samples, which is in line with the absence of metallic Au particles in their HRTEM images (Fig. 2A). The residual gold species in cyanide-leached Au/Al_2O_3 (0.16% Au) [46] and Au/CeO_2 (0.08% Au) [47] were also detected

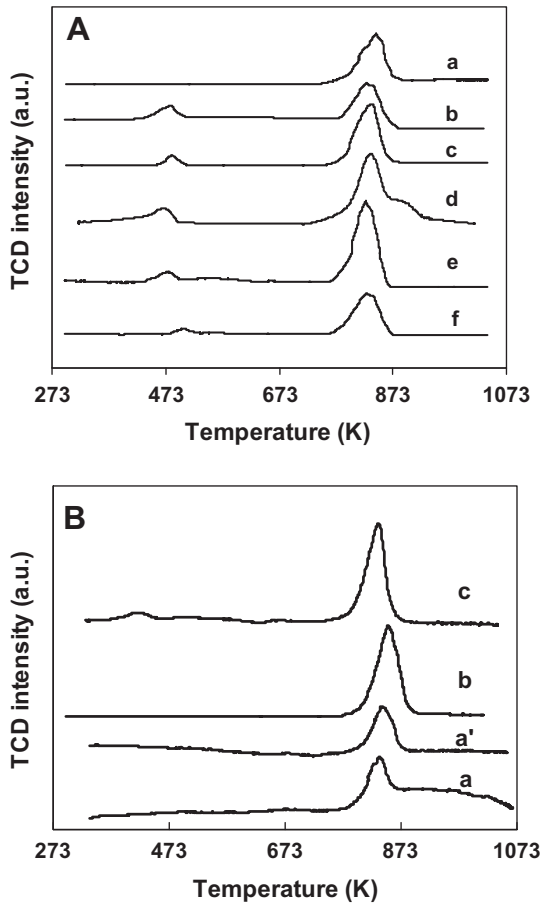

Fig. 5. TPR profiles of Au/ZrO_2-CP-673-*T* (A) and Au/ZrO_2-CP-1073-*T* (B) samples. *T* = 673 (a), 573 (b), 473 (c), and 393 K (d); (a′) denotes the water-treated Au/ZrO_2-CP-1073-673; (e) and (f) refer to 0.23% and 0.05%Au/ZrO_2-CP-673-473 samples.

as Au^{3+} ions by in situ EXAFS/XANES, though the exact nature of those gold cations in the cyanide-leached $Au/Ce(La)O_2$ samples remained unclear in Fu et al.'s work [29]. The lack of clear evidence of Au^+ ions in these supported gold catalysts with low gold loadings encouraged us to exclude any involvement of Au^+ ions in our Au/ZrO_2 samples. Thus, deconvolution of the XPS spectra in Fig. 4 was done based on the assumption that any gold species in Au/ZrO_2 catalysts would involve either metallic Au^0 atoms or cationic Au^{3+} ions. Although the BE shifts seemed too large in Fig. 4, the deconvolution resulted in two crossed doublets that are associated, respectively, with Au^{3+} ions (higher BEs) and Au^0 atoms (lower BEs) [27]. It is not surprising that the relative intensity of the doublet for Au^{3+} declined steadily with increasing catalyst calcination temperature *T*.

The reduction peak temperature, hydrogen consumption, and quantitative Au^{3+}/Au^0 ratio derived from the TPR measurements are summarized in Table 2. The peak temperature was lowered from 508 to 483 K when the gold loading was increased from 0.01% to 0.70% in the Au/ZrO_2-CP-673-473 samples, accompanied by concomitant decreases in the hydrogen consumption and Au^{3+}/Au^0 ratio. The Au^{3+}/Au^0 ratio for the Au/ZrO_2-CP-673-*T* samples (gold loading 0.7%) declined from 0.44 to 0 when *T* was increased from 393 to 673 K. These data are seemingly at variance with the much earlier work of Sermon et al. [11], who claimed that drying treatment of Au/SiO_2 and Au/Al_2O_3 catalysts containing less than 1.0 wt.% gold at a temperature as low as 393 K in either air or vacuum was sufficient to reduce their gold species to metallic gold. However, that earlier claim has not yet been confirmed, because it was based simply on the visual sample colors.

Fig. 5B shows the TPR profiles for Au/ZrO_2-CP-1073-*T* samples (gold loading 0.7%, *T* = 473–673 K). The water-treated Au/ZrO_2-CP-1073-673 was also subjected to TPR measurement, which is included as profile a'. Compared to those for Au/ZrO_2-CP-673-473 (Fig. 5A), the gold reduction peak shifted to a lower temperature (ca. 424 K) and the measured relative amount of Au^{3+} became as low as $Au^{3+}/Au^0 = 0.10$ for Au/ZrO_2-CP-1073-473 (Table 2). This comparison suggests that the fully dehydroxylated surface of ZrO_2-CP-1073 was inferior to that of -CP-673 for stabilizing the cationic gold species (Au^{3+} ions). No peak that was characteristic of Au^{3+} reduction was found on Au/ZrO_2-CP-1073-T samples at *T* = 573 and 673 K. The TPR profile for the water-treated sample appeared similar to that for its untreated counterpart, indicating that the water treatment and subsequent drying and calcination induced no change in the gold species. However, it seems that hydrogen reduction of the support material (from Zr^{4+} to Zr^{3+}) became more pronounced in the presence of Au^{3+} ions, as one could judge from the difference between profiles a and c. This would hint that the presence of Au^{3+} probably could promote the reduction of Zr^{4+} into Zr^{3+} via H_2 chemisorption.

XPS spectra analysis of the Au/ZrO_2 samples after the H_2-TPR measurement (Fig. S2) gave no signal for Zr^{3+} ions but only Zr^{4+} ions, with Zr3*d* BEs at 184.4 and 182.3 eV. The materials were then subjected to ESR measurement; the results are shown in Fig. 6. The Au/ZrO_2-CP-673-473 after H_2-TPR produced ESR signals at $g_\perp = 1.976$ and $g_{||} = 1.957$, which are indeed distinctive for Zr^{3+} ions. An additional ESR signal at $g = 2.003$ on this reduced sample signified formation of so-called F-centers (single electrons trapped in oxygen vacancies), which was frequently observed on reduced Au/ZrO_2 and Au/TiO_2 samples [45,48]. Surprisingly, a pair of ESR signals attributed to Zr^{3+} ions was also registered on both Au/ZrO_2-CP-673-473 and -673-673 samples. Similar signals were also recorded earlier on gold catalysts supported by mesoporous zirconia [45], as well as on zirconia nanoparticles with small sizes [49].

3.2.4. H_2 activation on Au/ZrO_2 catalysts

H_2-TPD experiments were performed to gain information about H_2 activation/dissociation at 393 K on the Au/ZrO_2 catalysts (Fig. 7). In order not to cause variation in the gold oxidation state, the samples were pretreated with flowing Ar, rather than H_2, at their calcination temperature (*T*). Two H_2-desorption peaks were detected for 0.05%Au/ZrO_2-CP-673-473 containing only isolated Au^{3+} ions, and Au/ZrO_2-CP-673-393 and -CP-673-473 containing Au^{3+} ions as well as Au^0 atoms. The peak in the low-temperature region (ca. 590–780 K) appeared much smaller than the peak in

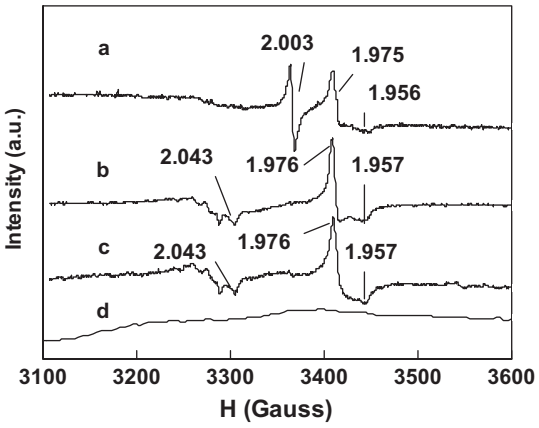

Fig. 6. ESR spectra measured at room temperature: (a) Au/ZrO_2-CP-673-473 after the H_2-TPR measurement; (b) Au/ZrO_2-CP-673-673; (c) Au/ZrO_2-CP-673-473; and (d) the blank (the empty tube).

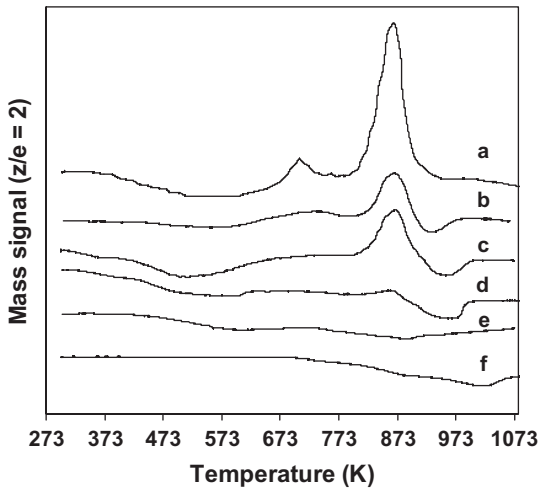

Fig. 7. H_2-TPD curves after the chemisorption of H_2 at 393 K over Au/ZrO_2-CP-673-*T* of *T* = 393 (b), 473 (c), and 673 K (d); (a), (e), and (f) refer to 0.05%Au/ZrO_2-CP-673-473, Au/ZrO_2-CP-1073-673, and ZrO_2-CP-673, respectively.

the high-temperature region (ca. 800–940 K). However, only a very small peak was detected in the high-temperature region for Au/ZrO_2-CP-673-673 containing only Au^0 atoms. Notably, hydrogen desorption was observed neither for OH-free ZrO_2-CP-1073 carrying Au particles nor for Au-free ZrO_2-CP-673 having surface OH-groups. It is deduced therefore that hydrogen activation in the absence of Au^{3+} ions would require some form of cooperation between metallic Au particles and ZrO_2-based hydroxyl groups.

3.3. Selective hydrogenation of 1,3-butadiene over Au/ZrO_2 catalysts

3.3.1. Effect of moisture and surface hydroxyl groups

Fig. 8 shows the effect of moisture (water vapor) in the reaction feed on the reaction rates for butadiene consumption normalized to the gold weight (i.e., mass-specific activity of gold) at 393 K over Au/ZrO_2-CP-673-673 and -CP-1073-673 catalysts. This figure registers a detrimental effect of moisture on the hydrogenation reaction of 1,3-butadiene for a wide range of moisture concentrations (20–6000 ppm). The reaction rate over Au/ZrO_2-CP-673-673 was lowered by 90% with the addition of ca. 6000 ppm moisture into the standard "dry" reaction feed. On the other hand, the same change in moisture concentration produced little effect on the reaction rate over Au/ZrO_2-CP-1073-673 catalyst (Au nanoparticles supported on a fully dehydroxylated ZrO_2), and the measured

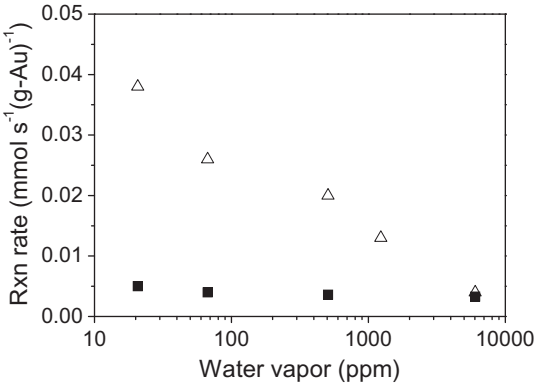

Fig. 8. Effect of water vapor (moisture) on the reaction rate by 1,3-butadiene consumption at 393 K over Au/ZrO_2-CP-*t*-673 of *t* = 673 (△) and 1073 K (■).

butadiene conversion levels were always no higher than that of the blank thermal reaction (2–3%).

Although the Au/ZrO_2-CP-1073-673 catalyst showed no activity in these experiments, remarkably enhanced activity was observed after the sample was treated with deionized water (Fig. 9). The conversion of 1,3-butadiene over the water-treated sample increased to 48.4%, which is one order of magnitude higher than that for the blank reaction (3.4%). However, the conversion of butadiene over this water-treated catalyst also decreased sharply when ca. 20 ppm moisture was introduced into the reaction feed. It should be pointed out that the "moisture-deactivated" catalyst could not be reactivated by switching the reaction feed off the moisture generator. Even in situ recalcination at 473 K in flowing air could only reactivate such a "moisture-deactivated" catalyst up to ca. 20% of its original activity. These results indicate that most of the active sites on the water-treated catalyst could be blocked or "destroyed" by the presence of added moisture. The adsorption energies of H_2O, H_2, and *trans*- and *cis*-1,3-butadiene on Au(1 1 1), according to a recent DFT calculation study [50], were −4.51, −0.81, −5.71, and −3.75 kcal/mol, respectively. This theoretical calculation would imply that the presence of moisture can not only block the gold sites for H_2 adsorption/activation but also compete with butadiene for the active gold sites during the hydrogenation reaction, if the hydrogenation activity is associated only with metallic gold.

Fig. 10 shows the reaction rate changes over Au/ZrO_2-CP-*t*-673 and -AN-*t*-673 catalysts with different *t*. The elevation of *t* from 673 up to 1073 K resulted in a pronounced and continuous decrease in the catalyst activity for both series of catalysts. As shown in Fig. 10 and Table 2, the average butadiene consumption rate and turnover frequency (TOF) based on exposed gold atoms within 6 h of TOS both decreased sharply with the increment of *t*. Notably, the conversion levels of butadiene over both Au/ZrO_2-CP-1073-673 and -AN-1073-673 were found no higher than that of the blank thermal reaction, implying that the metallic gold particles in both catalysts were essentially inactive for the hydrogenation reaction.

3.3.2. Effect of gold oxidation state

Fig. 11 shows the reaction rate changes over Au/ZrO_2-CP-673-*T* catalysts with varied *T*. The rates are 0.02, 0.10, 0.14, 0.20, and 0.38 mmol s^{-1} $(g\ Au)^{-1}$ for *T* = 773, 673, 573, 473, and 393 K, respectively. These data mean that the reaction rate decreased with a decline in the catalyst's Au^{3+}/Au^0 ratio when *T* varied between 393 and 673 K, since *T* elevation from 393 up to 673 K

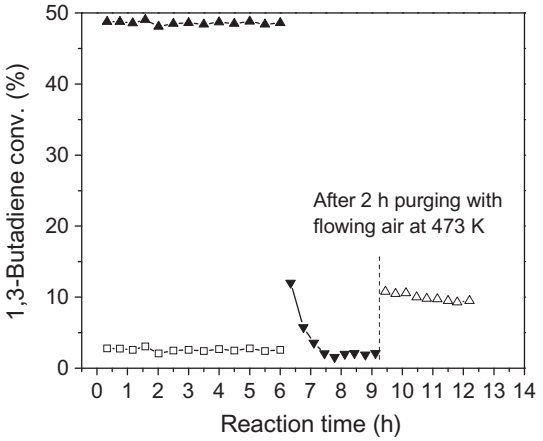

Fig. 9. Time course of 1,3-butadiene conversion over as-prepared Au/ZrO_2-CP-1073-673 (□) and its water-treated counterpart sample (▲). After 6 h, the reaction over the water-treated sample was continued by adding ca. 21 ppm moisture into the reaction feed gas (▼). The last set of data (△) shows the results with the standard "dry" reaction feed (without addition of moisture) after purging the reacted catalyst with flowing air for 2 h at 473 K.

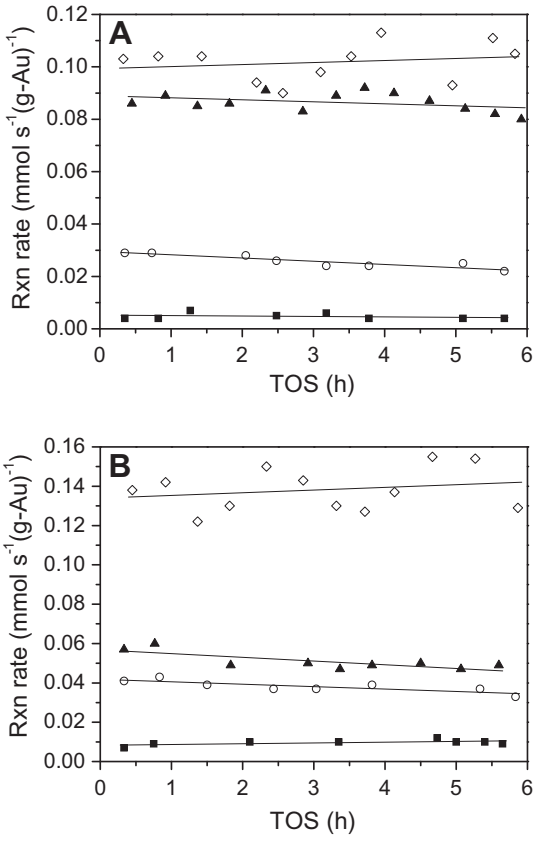

Fig. 10. Effect of support calcination temperature (t) on the reaction rates for 1,3-butadiene consumption by Au/ZrO_2-CP-t-673 (A) and Au/ZrO_2-AN-t-673 (B) of t = 673 (◇), 873 (▲), 973 (○), and 1073 K (■).

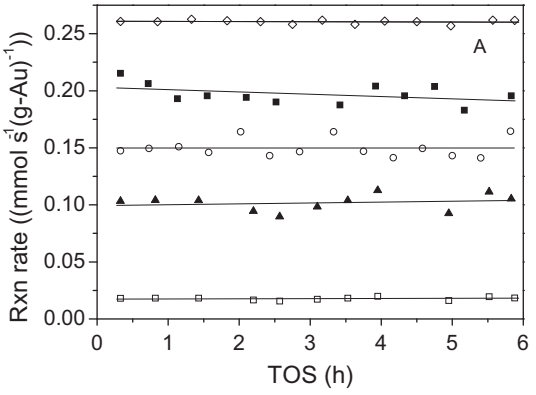

Fig. 11. Effect of catalyst calcination temperature (T) on the reaction rate for Au/ZrO_2-CP-673-T of T = 393 (◇), 473 (■), 573 (○), 673 (▲), and 773 K (□).

would cause Au^{3+} reduction and lower the Au^{3+}/Au^0 ratio from 0.42 to 0 (Table 2). The much lower activity of the T = 773 catalyst than of T = 673 was probably due to the loss of hydroxyl groups at the support surface as aforementioned.

Note that the butadiene conversion over the most active Au/ZrO_2-CP-673-393 was as high as 98.4% when the reaction was carried out with the "standard" reaction space velocity, GHSV = 8100 ml h^{-1} (g cat.)$^{-1}$ (Fig. S3). Such high butadiene conversion could heavily mask or undervalue the catalytic activity because the reaction deviated severely from the situation in a differential reactor. We therefore increased the feed space velocity to measure the reaction rate of this Au/ZrO_2-CP-673-393 catalyst. We observed a reversible variation in butadiene conversion between 98.4% and 61% when the feed GHSV was varied between 8100 and 19,200 ml h^{-1} (g cat.)$^{-1}$ (see Fig. S3). Specifically, the measured overall reaction rate was 0.26, 0.38, and 0.38 mmol s^{-1} (g Au)$^{-1}$, respectively, when the GHSV was 8100, 13,800, and 19,200 ml h^{-1} (g cat)$^{-1}$. The actual catalytic rate for this Au/ZrO_2-CP-673-393 catalyst is therefore 0.38 mmol s^{-1} (g Au)$^{-1}$, which is given in Table 2. It should be emphasized that the activity of Au/ZrO_2-CP-673-393 remained unchanged during the entire reaction period measured at 393 K (14 h, Fig. S3).

Fig. 12 shows the changes in butadiene conversion over Au/ZrO_2-CP-1073-T catalysts with varied T. The conversion over the T = 573 and 673 catalysts (2–3%) was no higher than that in the blank thermal reaction, much lower than that over the T = 473 catalyst (ca. 19%). As these two inactive catalysts contained only metallic Au nanoparticles, while the active T = 473 catalyst contained both Au^{3+} and Au^0, these results provide additional evidence for our finding that metallic gold particles supported on hydroxyl-free ZrO_2-CP-1073 possess no active sites for the hydrogenation reaction.

Considering that the function of Au^{3+} ions in the hydrogenation catalysis could be discounted or masked by possible involvement of zirconia-based hydroxyl groups, which would change with the t and T temperatures of a catalyst, we further investigated a series of m%Au/ZrO_2-CP-673-473 catalysts with lower gold loadings ($m \leqslant 0.7$). The preparation of these catalysts with invariant t and T temperatures could avoid, with the highest probability, changes in other properties of zirconia support (including hydroxyl groups, surface area, and crystalline phase). It is shown in Fig. 13 that the butadiene conversion (ca. 50%) over 0.05%Au/ZrO_2-CP-673-473 was higher than that (ca. 40%) over 0.23% Au/ZrO_2-CP-673-473 catalyst, though the gold loading in the later catalyst was about four times higher. The measured average reaction rates (within 6 h TOS) were 2.01, 0.34, and 0.20 mmol s^{-1} (g Au)$^{-1}$ for 0.05%, 0.23%, and 0.76%Au/ZrO_2-CP-673-473 catalysts with $Au^{3+}/Au^0 = \infty$ (infinity), 0.83, and 0.33, respectively (Table 2). Notably, the reaction rates and TOFs remained the same for the catalysts containing 0.05% and 0.01% gold, showing that the isolated Au^{3+} ions in these two samples were equally active for the hydrogenation reaction.

Fig. 13 also compares the performance of 0.76%Au/ZrO_2-CP-673-473 with its cyanide-leached counterpart (0.08%Au/ZrO_2-CP-673-473). The cyanide-leached catalyst with only 0.08% gold in the Au^{3+} state surprisingly demonstrated much higher activity [31]. Specifically, the reaction rate and TOF for the cyanide-leached catalyst were enhanced to 2.15 mmol s^{-1} (g Au)$^{-1}$ and 0.42 s^{-1} from 0.20 mmol s^{-1} (g Au)$^{-1}$ and 0.17 s^{-1} for the unleached

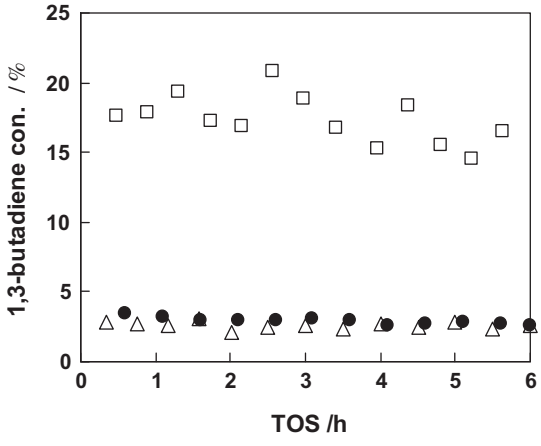

Fig. 12. Effect of catalyst calcination temperature (T) on butadiene conversion for Au/ZrO_2-CP-1073-T at T = 473 (□), 573 (●), and 673 K (Δ).

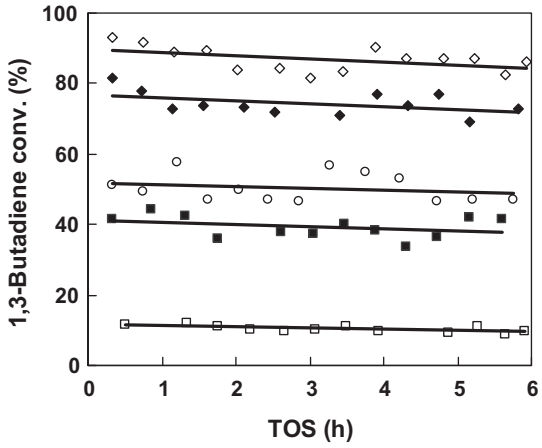

Fig. 13. Effect of gold loading on 1,3-butadiene conversion at 393 K over Au/ZrO_2-CP-673-473 containing 0.76 (♦), 0.23 (■), 0.08 (◇), 0.05 (○), and 0.01% Au (□).

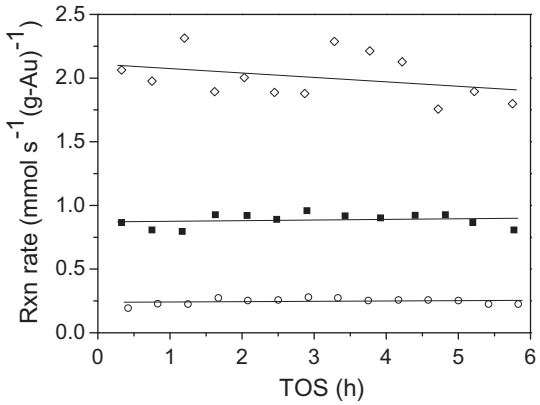

Fig. 14. Effect of reduction pretreatment on the reaction rate over 0.05%Au/ZrO_2-CP-673-473 catalyst: (◇) 473 K in Ar, (■) 473 K in H_2, (○) 523 K in H_2.

catalyst. For the hydrogenation of 1-pentene over Au/SiO_2, Sermon et al. [11] also found that the activity of gold increased remarkably when the gold loading was lowered to less than 0.1% (e.g., 0.01% or 0.05%). The active gold species in those Au/SiO_2 catalysts could most possibly be Au^{3+} rather than Au^0.

Interestingly, the reaction over the Au/ZrO_2-CP-673-473 catalysts with various gold loadings was found to be 100% selective for butenes (Fig. S4); no butane was detected even over the most active 0.08% Au/ZrO_2-CP-673-473 catalyst (butadiene conversion 85.4%). The thermodynamic equilibrium composition of butenes at 393 K is calculated to be 8.3%, 63.8%, and 27.8% for 1-butene, *trans-2*-butene, and *cis-2*-butene. The quantity of the major component of butenes obtained in the present study (ca. 60% 1-butene) is much higher than the value predicted from the thermodynamic equilibrium composition of butenes. The high concentration of 1-butene could indicate that the hydrogenation of 1,3-butadiene on Au/ZrO_2 catalysts mainly occurs according to the 1,2-addition pathway, which is a feature markedly different from thermal hydrogenation via 1,4-addition to trans-2-butene as the main product [19]. The *trans*/*cis* ratio of 2-butenes was in the range 0.3–1.0 over all Au/ZrO_2 catalysts, which is lower than the ratio of 1.5–2 (close to the equilibrium value) obtained over Pt and other Group VIII noble metals [19]. According to a mechanism proposed by Meyer and Burwell [51], the semihydrogenated 1,3-butadiene would be adsorbed either as *syn*- or *anti*-π-allyl species. The ratio of these two surface intermediates should be close to that in the gas phase, which is about 1:10 [19]. If this was the case, the interconversion from an *anti* to a *syn* intermediate would occur easily on Au/ZrO_2, resulting in a low proportion of *trans*-2-butene. This would mean kinetically favorable *trans*- to *cis*- isomerization during the reaction over a gold catalyst [52].

The key role of Au^{3+} ions in determining the hydrogenation activity was further confirmed by investigating the effect of hydrogen reduction on the catalytic activity of 0.05%Au/ZrO_2-CP-673-473 (Fig. 14). H_2-reduction pretreatment at 473 K led to a sharp decrease in the reaction rate (from ca. 2.01 to 0.88 mmol s^{-1} (g Au)$^{-1}$), and complete reduction of Au^{3+} ions at 523 K further decreased the rate to 0.24 mmol s^{-1} (g Au)$^{-1}$. These results clearly suggest that the catalyst suffered severe activity losses after the reduction of Au^{3+} ions.

4. Discussion

The present data demonstrate that the Au^{3+}/Au^0 ratio, ZrO_2-based hydroxyl groups, and moisture in the reaction feed are important factors to the catalytic activity of a Au/ZrO_2 catalyst for the hydrogenation of 1,3-butadiene. The former two factors were not always independent and were sensitively related to the gold loading, the calcination temperature of ZrO_2 before gold loading (t), and the catalyst calcination temperature (T).

All of the present Au/ZrO_2 catalysts except the cyanide-treated one were prepared by deposition–precipitation at pH 9.0. The dominant gold species in solution would be $Au(OH)_4^-$ and/or $AuCl(OH)_3^-$ [53] and the surface of the ZrO_2 support would carry negative charges, as its isoelectronic point is pH 6.7. Scheme 1 is proposed to illustrate possible interactions of $Au(OH)_4^-$ at the surface. The deposition of $Au(OH)_4^-$ would lead to surface gold oxyhydroxide or hydroxyl gold species (e.g., AuO(OH) and/or $Au(OH)_3$). These species could easily dehydrate to give Au_2O_3 at 413–423 K. This latter product would then decompose to give metallic Au when calcined at slightly higher temperatures; decomposition of unsupported gold oxides to metallic Au occurred even at 353 K [2]. Thus, the presence of unreduced Au^{3+} ions in our samples would be associated with oxy-gold species, such as AuO(OH), $Au(OH)_3$, or Au_2O_3, stabilized on the support surface [26,27,31,43].

When the gold loading on ZrO_2-CP-673 (120 m^2/g) was lowered from 0.76% to 0.23% and then 0.08%, the density of gold atoms at the support surface would decrease from 19.4 to 5.9 and then 2.1 gold atoms per 100 nm^2. The lower density of gold atoms on the support surface would probably limit the sintering and Ostwald ripening of gold [53], which accounts for the observed increase in the average Au particle size with increasing gold loading. The addition of gold titrated, in a sense, the stronger binding sites and then weaker ones on the support surface. Thus, the oxy-gold species at very low gold loadings (e.g., <0.1%) would be strongly bound and their decomposition or reduction to Au^0 would require some higher temperatures. This issue is supported by our present data (Fig. 5) that the Au^{3+}/Au^0 ratio and TPR peak temperature for Au^{3+} reduction both declined with increasing gold loading for the *m*%Au/ZrO_2-CP-673-473 samples (Table 2). A recent DFT calculation study showed that isolated Au^{3+} ions on a stepped ZrO_2 surface are more stable than those on a flat surface [54].

Due to the much lower surface area (14 m^2/g) and concentration of hydroxyl groups for ZrO_2-CP-1073, compared with ZrO_2-CP-673, the density of gold atoms at the support surface increased to as high as 158 per 100 nm^2 in the Au/ZrO_2-CP-1073-*T* samples. This would significantly reduce the stability of cationic gold species while at the same time increasing the probability of gold sintering during the catalyst preparation (Scheme 1), leading to lower Au^{3+}/Au^0 ratios and larger Au particle sizes for the Au/ZrO_2-CP-1073-*T* catalysts.

Differences in the size and size distribution of Au and ZrO_2 nanoparticles could also influence their activity, as documented

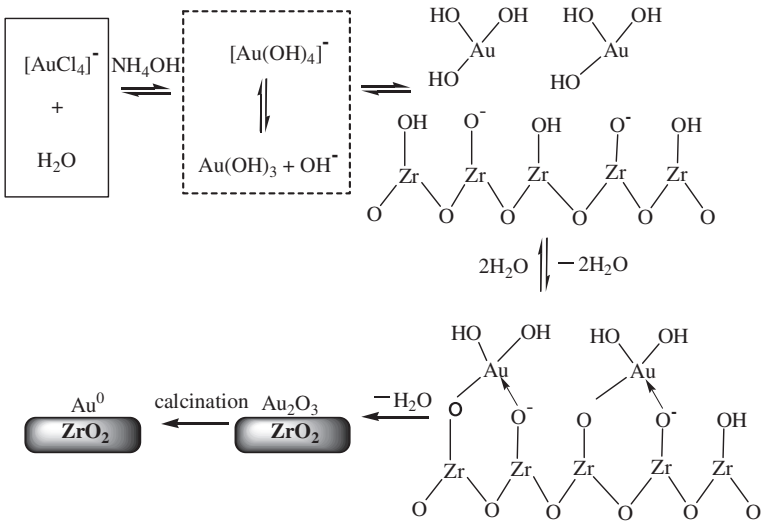

Scheme 1. Possible interaction of $Au(OH)_4^-$ ions with the negatively charged ZrO_2 surface and their subsequent transformations during catalyst preparation.

for CO oxidation [1–6]. Okumura et al. [12] found that the activity of Au/Al_2O_3 catalysts for butadiene hydrogenation was almost insensitive to the size of Au nanoparticles (2.5–37.0 nm). In the work of Hugon et al. [55], the TOF rates on exposed Au^0 atoms in both Au/TiO_2 and Au/Al_2O_3 catalysts for butadiene hydrogenation also varied slightly (within a factor of 1.3) when the average Au particle size changed from 5 to 2 nm. By changing the calcination temperature (373–923 K) of an Au/Al_2O_3 catalyst to effect changes in the Au particle size, Jia et al. [13] observed that the optimum Au particle size for the hydrogenation of acetylene was ca. 3 nm. However, these authors made no consideration of the possible involvement of oxy-gold species and surface hydroxyl groups. By carefully controlling the size of metallic Au particles (average 4–5 nm) on ZrO_2-AN-*t* support, the catalytic activity of Au/ZrO_2-AN-*t*-673 also decreased with increasing *t* (see Fig. 10B and Table 2). So the sizes of Au nanoparticles in Au/ZrO_2-CP-*t* catalysts would not be a main cause for the sharp decrease in the TOF from 0.12 to 0.01 s^{-1} when *t* was increased from 673 to 1073 K (Table 2).

At the present stage, it remains difficult to decouple the two effects on gold activity when they coexist: hydroxyl groups and nanosize of ZrO_2 particles. Obviously, the Au–ZrO_2 contact boundary or interface would increase with the decline in ZrO_2 particle size if Au particles could be made in similar sizes. In this sense, the Au–ZrO_2 interface would be maximized in nanocomposite Au/ZrO_2-AN-673-673 composed of comparably sized Au (4–5 nm) and ZrO_2-AN-673 (5–10 nm) particles [5]. Those metallic gold atoms in close contact with the ZrO_2 support or located at the Au–ZrO_2 interface have proven to be the catalytic active sites for CO oxidation [1,2,5], and H_2–D_2 exchange reactions [22]. At first glance, the obtaining of the highest 1,3-butadiene conversion (49.0%) and specific rate (0.13 mmol s^{-1} (g Au)$^{-1}$) on Au/ZrO_2-AN-673-673 among all of the Au/ZrO_2-AN-*t*-673 and -CP-*t*-673 catalysts ($673 \leqslant t \leqslant 1073$ K) could indicate a possible nanosize effect of the support particles on the activity of Au particles [56]. In this case, the slightly higher activity of Au/ZrO_2-AN-973-673 than of Au/ZrO_2-CP-973-673 was explicable by the smaller average size of ZrO_2 particles in the former. Nevertheless, Au/ZrO_2-AN-873-673 with smaller ZrO_2 particles compared to Au/ZrO_2-CP-873-673 exhibited lower activity, which indicates that the higher concentration of hydroxyl groups in the latter catalyst could outweigh the inferiority of larger ZrO_2 particles.

The Au^{3+}-free metallic Au nanoparticles supported on OH-free ZrO_2 (ZrO_2-CP-1073 of 40–200 nm and ZrO_2-AN-1073 of 25–40 nm) or in Au/ZrO_2-CP-1073-673 and -AN-1073-673 catalysts appeared inactive for butadiene hydrogenation but became remarkably active after being subjected to a water treatment (e.g., Fig. 9). This kind of catalyst "activation" by water treatment did not involve any Au^{3+}, as the TPR measurement detected no formation of Au^{3+} ions in the water-treated sample (Fig. 5B). These results would instead indicate that the size of the zirconia support was not among the keys to the hydrogenation activity. Therefore, the remarkably enhanced activity after the water treatment should be associated with the partial regeneration of hydroxyl groups on the ZrO_2 surface, as indicated by the IR and TG measurements, which convincingly demonstrates the vital role of the surface hydroxyl groups in the hydrogenation of 1,3-butadiene.

OH groups on ZrO_2 were proposed to supply protons, either directly or indirectly [57,58]. However, H/D exchange reactions between D_2 and the OH groups occurred only at above 323 K [59], giving a maximum H/D exchange rate at 418 K [60]. Indeed, both butadiene hydrogenation and H_2/D_2 exchange reactions were observed using a closed recirculation reactor at 323–348 K on "pure" ZrO_2 catalysts pretreated at varying temperatures (673–1173 K) [61]. The specific surface reaction rates for both reactions increased with increasing catalyst pretreatment temperature up to 873 K. However, the catalytic rates declined with further increase of the pretreatment temperature and became zero when the pretreatment temperature was elevated to 1073 K or higher. These earlier data [61] could imply that the surface hydroxyl groups could be a key to H_2 activation on zirconia. By using a H_2/D_2 mixture for butadiene hydrogenation, Buchanan and Webb [10] found earlier that the activation of H_2/D_2 on Au/Al_2O_3 catalysts would involve a hydrogen source (surface OH groups) on the γ-Al_2O_3 support, and metallic Au particles on OH-free α-Al_2O_3 support were inactive for the hydrogenation reaction. Recently, metallic Au clusters on partially dehydroxylated MgO (pretreated in vacuum at 673 K) were also found inactive in ethylene hydrogenation [30].

In this study, nanosized ZrO_2 powders without gold showed no activity for the hydrogenation reaction. The TOF data for butadiene consumption based on exposed Au^0 atoms over our Au/ZrO_2 catalysts were in the range of 0.01–0.12 s^{-1} (Table 2). These data are close to those (ca. 0.01–0.09 s^{-1}) at 423 K for the Au/TiO_2 and Au/Al_2O_3 catalysts under similar reaction conditions [12]. Gluhoi et al. [62] showed that the D/H exchange rate between D_2 and the surface hydroxyl groups of γ-Al_2O_3 was significantly enhanced when the oxide (γ-Al_2O_3) was loaded with nanosized Au particles.

Thus, it can be argued that the presence of metallic Au particles can promote the activation/dissociation of H_2 on OH-carrying ZrO_2 surfaces. Indeed, our H_2-TPD experiments evidenced that the presence of Au particles improved the chemisorption of H_2, since a weak H_2-desorption peak was detected for Au/ZrO_2-CP-673-673 but not for ZrO_2-CP-673 (Fig. 7d and f). Au/ZrO_2-CP-1073-673 with no surface OH-groups was also inactive for H_2 chemisorption. In a catalyst containing no Au^{3+} ions, the metallic Au particles and the OH-carrying ZrO_2 have to work together for H_2 activation.

The Au/ZrO_2 catalysts summarized in Table 2 can be grouped into four categories. The Au/ZrO_2-CP-1073-673 and -AN-1073-673 catalysts, which feature metallic gold particles supported on an OH-free ZrO_2 surface as depicted in Scheme 2a, are ascribed to the first category. The surface Au^0 atoms in these catalysts were essentially inactive for the selective hydrogenation of 1,3-butadiene, as in the cases of OH-free Au/α-Al_2O_3 for the H/D exchange reaction [10] and dehydroxylated Au/MgO for the hydrogenation of ethene [30]. Therefore, metallic Au nanoparticles on OH free ZrO_2 surfaces are unlikely to possess active sites for H_2 activation/dissociation. The surface of these Au particles resembles those of bulk Au in that they show no activity for H_2 dissociation [21]. This explanation is further supported by our observation that the Au/ZrO_2-CP-1073-673 catalyst showed no activity for H_2 chemisorption, as revealed by the H_2-TPD data (Fig. 7e).

The Au/ZrO_2-CP-*t*-*T* and -AN-*t*-*T* catalysts ($t < 1073$ K) with $T = 673$ or 773 K, which feature metallic Au nanoparticles supported on ZrO_2 surface with more or less residual OH-groups (see Scheme 2b), are assigned to the second category. It should be pointed out that the catalysts in this category have been the subject of many investigations. A number of models have been proposed toward understanding of the catalytically active gold sites for the hydrogenation catalysis [9,10,12,23,63]. Exposed metallic gold atoms were proposed to be the active sites in most cases, including those on very small Au clusters not sensed by TEM [9] or less than 2 nm [23], low-coordinated edge or corner atoms at the surfaces of Au nanoparticles [12,63]. However, a model proposed by Buchanan and Webb [10] claimed that the active sites responsible for H_2 activation were originated from the oxide (γ-Al_2O_3) support surface but not the Au particles. Our data clearly show that even so, interaction between metallic Au particles and zirconia can be important to the H_2 activation on the Au/ZrO_2 catalysts; participation of surface hydroxyl groups is, however, quite indispensable. A solid piece of evidence for this argument is our observation that the inactive Au/ZrO_2-CP-1073-673 catalyst can also become highly active after it is subjected to simple water treatment (Fig. 9). In a very recent report of Fujitani et al. [23], the activity of Au/TiO_2 for H_2 dissociation could be related to the number of Au^0 atoms located at the circumference of the supported Au particles. This does not violate our point that H_2 activation in the absence of Au^{3+} ions would need cooperation between the Au particles and the oxide-based OH groups, since it does not exclude the possibility that some OH groups residing in the support oxide (TiO_2) could be also involved in the H_2 dissociation chemistry.

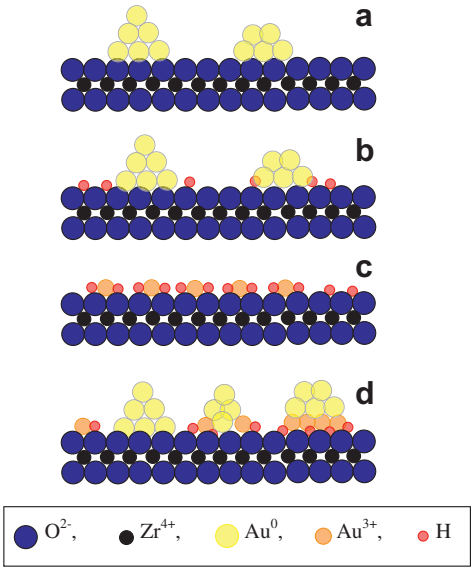

Scheme 2. Proposed structure models for Au/ZrO_2 catalysts: (a) metallic Au^0 particles deposited on OH-free ZrO_2-CP-1073 or ZrO_2-AN-1073; (b) metallic Au^0 particles deposited on OH-carrying ZrO_2; (c) immobilized isolated Au^{3+} species on ZrO_2; (d) dispersed Au^0 particles and Au^{3+} species on ZrO_2 with varying OH concentrations.

Au/ZrO_2 catalysts containing no more than 0.08% Au, which feature isolated Au^{3+} ions on the support surface (Scheme 2c), are ascribed to the third category. The isolated Au^{3+} in the catalysts of this category could be surface immobilized AuO(OH) or $Au(OH)_3$ [50]; they showed the same highest catalytic activity by the reaction rate (2.1 mmol s^{-1} (g Au)$^{-1}$) and TOF (0.41 s^{-1}), despite their varied gold loadings (0.01–0.08%). As we have discussed earlier [27,31], these results suggest that the isolated Au^{3+} ions are equally active for the hydrogenation of 1,3-butadiene. It should be pointed out that the reaction rate and TOF of these isolated Au^{3+} ions were 1–2 orders of magnitude higher than those of the Au particles in the samples of the second category (Table 2). The TOF of these isolated Au^{3+} ions is even comparable to those of Group VIII noble metal catalysts (e.g., 0.2–1.0 s^{-1} for supported Pd catalysts) [19]. The remarkable difference in activity by TOF between these surface-type Au^{3+} ions and Au^0 atoms could mean different mechanisms for the required dissociative activation of H_2. DFT calculations [21,54] indicate that H_2 dissociation on cationic gold species would be easy, although metallic Au^0 atoms are noble to H_2 chemisorption. The capability of surface Au^{3+} ions for H_2 activation was clearly evidenced in our H_2-TPD experiments, where the amount of chemisorbed hydrogen was sensitively related to the sample Au^{3+}/Au^0 ratio (Fig. 7).

The catalysts in the fourth category include 0.23% Au/ZrO_2-CP-673-473 and Au/ZrO_2-CP-673-*T* with $T = 393$, 473, and 573 K, which feature coexisting Au^0 atoms and Au^{3+} ions on OH-carrying ZrO_2 surface (Scheme 2d). These catalysts may be regarded as mixtures of the catalysts in categories 2 and 3 in varying proportions. There are thus three types of surface sites for H_2 activation/dissociation on the catalysts of this category, one being at the interfaces between the Au nanoparticles and the OH-carrying ZrO_2, the second being the isolated surface Au^{3+} ions, and the third involving ensembles of Au^0 atoms and Au^{3+} ions on the OH-carrying ZrO_2 surface. This third type of catalytic sites was also proposed previously to operate in gold-catalyzed CO oxidation reactions [3,64] but had not yet been considered in gold-catalyzed hydrogenation reactions. For the catalysts in this category, the TOF data based on exposed Au^0 atoms (numbers outside the parentheses in Table 2) appeared not very different from those based on the Au^{3+} ions (numbers inside the parentheses in Table 2). However, the activity of these Au^{3+} ions by TOF (0.16–0.25 s^{-1}) is much lower than that (0.41 s^{-1}) of the isolated Au^{3+} ions in the catalysts of the third category (Table 2 and Fig. 13). This difference could hint that the Au^0 atoms could lower the catalytic activity of their coexisting Au^{3+} ions, either by burying some of the Au^{3+} ions or by electronic interaction [27].

Scheme 3 is proposed to highlight the richness of catalytic sites for hydrogen activation and their subsequent reaction with 1,3-butadiene over Au/ZrO_2 catalysts. Though little information is available at this stage for the adsorption of 1,3-butadiene, this substrate would become adsorbed by nucleophilic interaction via

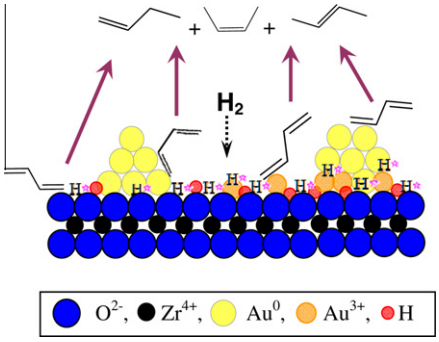

Scheme 3. Proposed reaction routes over zirconia-supported gold catalyst for the selective hydrogenation of 1,3-butadiene. *Note*: the activated hydrogen atoms are shown as the H☆ species.

either C=C bonds with the surface Au^0 and/or Au^{3+} sites [10,52], or Zr^{4+} or Zr^{3+} sites at the surface of zirconia [61]. Further reaction between the adsorbed butadiene and the activated hydrogen produces the product butenes.

The stability of surface Au^{3+} ions in the reducing atmosphere of the hydrogenation reaction can be critical for applications. The slightly changed catalytic rates, as observed in Figs. 11 and 13, and Fig. S3, would demonstrate that the active Au^{3+} ions in our catalysts were stable enough to survive the reaction. Our TPR data (Fig. 5) evidenced that the onset reduction temperature for the Au^{3+} ions was always higher than the reaction temperature (393 K). Stabilization of Au^{3+} ions by interaction with the support oxide was also documented in the literature, especially when CeO_2 [28,29] and ZrO_2 [45,65] were used as the support oxides. Our quantitative TPR measurement revealed that the quantity of Au^{3+} ions in the Au/ZrO_2-CP-673-473 catalyst did not change after it was used to catalyze the hydrogenation reaction for 6 h. This is a piece of strong evidence for the catalytic stability of Au^{3+} ions in the hydrogenation reaction.

5. Conclusions

This work shows that the gold oxidation state and hydroxyl groups on the support oxide surface played vital roles in hydrogenation catalysis by Au/ZrO_2. A continued activity decrease is seen when the density of surface hydroxyl groups is lowered by elevating the pre-calcination temperature of ZrO_2. Au nanoparticles supported on OH-free ZrO_2 are inactive, but become highly active after they are subjected to a simple water treatment. Catalytic ensembles involving metallic Au^0 atoms and Au^{3+} ions on OH-carrying ZrO_2 have been proposed to address the structural features of active sites in these Au/ZrO_2 catalysts for H_2 activation.

Acknowledgment

We thank the NSF of China (20921001 and 20903119) and the Program for New Century Excellent Talents in University (NCET) for financial support.

Appendix A. Supplementary material

Supplementary data associated with this article can be found, in the online version, at doi:10.1016/j.jcat.2011.01.002.

References

[1] G.C. Bond, C. Louis, D.T. Thompson (Eds.), Catalysis Science Series 6, Catalysis by Gold, Imperial College Press, United Kingdom, 2006. p. 1.
[2] M. Haruta, S. Tsubota, T. Kobayashi, H. Kageyama, M.J. Genet, B. Delmon, J. Catal. 144 (1993) 175.
[3] G.C. Bond, D.T. Thompson, Gold Bull. 33 (2000) 41.
[4] M.C. Kung, R.J. Davis, H.H. Kung, J. Phys. Chem. C 111 (2007) 11767.
[5] X. Zhang, H. Wang, B.-Q. Xu, J. Phys. Chem. B 109 (2005) 9678.
[6] M.S. Chen, D.W. Goodman, Catal. Today 111 (2006) 22.
[7] P. Claus, Appl. Catal. A 291 (2005) 222.
[8] A. Comas-Vives, C. Gonzalez-Arellano, A. Corma, M. Iglesias, F. Sánchez, G. Ujaque, J. Am. Chem. Soc. 128 (2006) 4756.
[9] G.C. Bond, P.A. Sermon, G. Webb, D.A. Buchanan, P.B. Wells, J. Chem. Soc. Chem. Commun. (1973) 444.
[10] D.A. Buchanan, G. Webb, J. Chem. Soc. Faraday Trans. 71 (1975) 134.
[11] P.A. Sermon, G.C. Bond, P.B. Wells, J. Chem. Soc. Faraday Trans. 75 (1979) 385.
[12] M. Okumura, T. Akita, M. Haruta, Catal. Today 74 (2002) 265.
[13] J. Jia, K. Haraki, J.N. Kondo, K. Domen, K. Tamaru, J. Phys. Chem. B 104 (2000) 11153.
[14] J.E. Bailie, G.J. Hutchings, Chem. Commun. (1999) 2151.
[15] J.E. Bailie, H.A. Abdullah, J.A. Anderson, C.H. Rochester, N.V. Richardson, N. Hodge, J.-G. Zhang, A. Burrows, C.J. Kiely, G.J. Hutchings, Phys. Chem. Chem. Phys. 3 (2001) 4113.
[16] J.E. Bailie, G.J. Hutchings, Catal. Commun. 2 (2001) 291.
[17] C. Mohr, H. Hofmeister, P. Claus, J. Catal. 213 (2003) 86.
[18] H. Shi, N. Xu, D. Zhao, B.-Q. Xu, Catal. Commun. 9 (2008) 1949.
[19] H. Arnold, F. Döbert, J. Gaube, in: G. Ertl, H. Knözinger, J. Weitkamp (Eds.), Handbook of Heterogeneous Catalysis, vol. 5, VCH Weinheim, 1997, p. 2165.
[20] S. Lin, M.A. Vannice, Catal. Lett. 10 (1991) 47.
[21] B. Hammer, J.K. Norskov, Nature 376 (1995) 238.
[22] S.A. Varganov, R.M. Olson, M.S. Gordon, G. Mills, H. Metiu, J. Chem. Phys. 120 (2004) 5169.
[23] T. Fujitani, I. Nakamura, T. Akita, M. Okumura, M. Haruta, Angew. Chem. Int. Ed. 48 (2009) 9515.
[24] M. Boronat, F. Illas, A. Corma, J. Phys. Chem. A 113 (2009) 3750.
[25] G.J. Hutchings, M.S. Hall, A.F. Carley, P. Landon, B.E. Solsona, C.J. Kiely, A. Herzing, M. Makkee, J.A. Moulijn, A. Overweg, J.C. Fierro-Gonzalez, J. Guzman, B.C. Gates, J. Catal. 242 (2006) 71.
[26] E.D. Park, J.S. Lee, J. Catal. 186 (1999) 1.
[27] X. Zhang, H. Shi, B.-Q. Xu, Catal. Today 122 (2007) 330.
[28] S. Carrettin, A. Corma, M. Iglesias, F. Sánchez, Appl. Catal. A 291 (2005) 247.
[29] Q. Fu, H. Saltsburg, M. Flytzani-Stephanopoulos, Science 301 (2003) 935.
[30] J. Guzman, B.C. Gates, J. Catal. 226 (2004) 111.
[31] X. Zhang, H. Shi, B.-Q. Xu, Angew. Chem. Int. Ed. 44 (2005) 7132.
[32] X. Zhang, H. Shi, B.-Q. Xu, Science and Technology in Catalysis 2006, in: K. Eguchi, M. Machida, I. Yamanaka, Eds., Kondansha-Elsevier, Stud. Surf. Sci. Catal., vol. 172, 2007, p. 481.
[33] M. Daté, M. Haruta, J. Catal. 201 (2001) 221.
[34] C.K. Costello, J.H. Yang, H.Y. Law, Y. Wang, J.N. Lin, L.D. Marks, M.C. Kung, H.H. Kung, Appl. Catal. A 243 (2003) 15.
[35] B.-Q. Xu, J.-M. Wei, J.-L. Li, Q.-M. Zhu, Top. Catal. 22 (2003) 77.
[36] J. Kondo, Y. Sakata, K. Domen, K. Maruya, T. Onishi, J. Chem. Soc. Faraday Trans. 86 (1990) 397.
[37] G.K. Chuah, S. Jaenicke, B.K. Pong, J. Catal. 175 (1998) 80.
[38] S.L. Jones, C.J. Norman, J. Am. Ceram. Soc. 71 (1988) C190.
[39] Y. Nakano, T. Iizuka, H. Hattori, K. Tanabe, J. Catal. 57 (1978) 1.
[40] L.L. Hench, J.K. West, Chem. Rev. 90 (1991) 33.
[41] K.T. Jung, A.T. Bell, J. Mol. Catal. A 163 (2000) 27.
[42] M.G. Mason, Phys. Rev. B 27 (1983) 748.
[43] N.A. Hodge, C.J. Kiely, R. Whyman, M.R.H. Siddiqui, G.J. Hutchings, Q.A. Pankhurst, F.E. Wagner, R.R. Rajaram, S.E. Golunski, Catal. Today 72 (2002) 133.
[44] J. Guzman, B.C. Gates, J. Phys. Chem. B 107 (2003) 2242.
[45] L. Ilieva, J.W. Sobczak, M. Manzoli, B.L. Su, D. Andreeva, Appl. Catal. A 291 (2005) 85.
[46] J.T. Calla, R.J. Davis, Catal. Lett. 99 (2005) 21.
[47] Y. Guan, E.J.M. Hensen, Phys. Chem. Chem. Phys. 11 (2009) 9578.
[48] P. Claus, A. Brücker, C. Mohr, H. Hofmeister, J. Am. Chem. Soc. 122 (2000) 11430.
[49] H. Liu, L. Feng, X. Zhang, Q. Xue, J. Phys. Chem. 99 (1995) 332.
[50] L. Zhao, H. Liu, W. Bu, J. Gao, C. Xu, X. Zhang, Y. Chen, Function of Water for the Adsorption of H_2 and 1,3-butadiene on Au (1 1 1): A DFT Study, unpublished results.
[51] E.F. Meyer, R.L. Burwell, J. Am. Chem. Soc. 85 (1963) 2881.
[52] X.F. Yang, A.Q. Wang, Y.L. Wang, T. Zhang, J. Li, J. Phys. Chem. C 114 (2010) 3131.
[53] F. Moreau, G.C. Bond, A.O. Taylor, J. Catal. 231 (2005) 105.
[54] Z.P. Liu, C.M. Wang, K.N. Fan, Angew. Chem. Int. Ed. 45 (2006) 6865.
[55] A. Hugon, L. Delannoy, C. Louis, Gold Bull. 41 (2008) 127.
[56] X. Zhang, B.-Q. Xu, Chem. J. Chin. Univ. 26 (2005) 106.
[57] T. Onishi, H. Abe, K. Maruya, K. Domen, J. Chem. Soc. Chem. Commun. 9 (1985) 617.
[58] J. Kondo, K. Domen, K. Maruya, T. Onishi, Chem. Phys. Lett. 188 (1992) 443.
[59] K. Tanabe, Mater. Chem. Phys. 13 (1985) 347.
[60] D. Martin, D. Duprez, J. Phys. Chem. B 101 (1997) 4428.
[61] Y. Nakano, T. Yamaguchi, K. Tanabe, J. Catal. 80 (1983) 307.
[62] A.C. Gluhoi, H.S. Vreeburg, J.W. Bakker, B.E. Nieuwenhuys, Appl. Catal. A 291 (2005) 145.
[63] E. Bus, J.T. Miller, J.A. van Bokhoven, J. Phys. Chem. B 109 (2005) 14581.
[64] H.H. Kung, M.C. Kung, C.K. Costello, J. Catal. 216 (2003) 425.
[65] X. Zhang, A. Corma, Angew. Chem. Int. Ed. 47 (2008) 4358.